Ocean Dynamics

A new instability mechanism related to high-angle waves

--Manuscript Draft--

Manuscript Number:	
Full Title:	A new instability mechanism related to high-angle waves
Article Type:	Topical Collection - CoastDyn 2017
Keywords:	coastal geomorphology; self-organized patterns; high-angle waves; shore-oblique sand bars
Corresponding Author:	Albert Falques, Ph.D Universitat Politecnica de Catalunya Barcelona, Barcelona SPAIN
Corresponding Author Secondary Information:	
Corresponding Author's Institution:	Universitat Politecnica de Catalunya
Corresponding Author's Secondary Institution:	
First Author:	Albert Falques, Ph.D
First Author Secondary Information:	
Order of Authors:	Albert Falques, Ph.D
	Nabil Kakeh
	Daniel Calvete
Order of Authors Secondary Information:	
Funding Information:	Secretaría de Estado de Investigación, Desarrollo e Innovación (CTM2015-66225-C2-1-P) — Prof Albert Falques
Abstract:	For wave incidence angles at breaking above approx. 45 degrees the one-line approximation of coastal dynamics predicts an unstable shoreline giving rise to the formation of self-organized sand waves. This instability (EHAWI) is scale-free and the growthrate increases without bound for decreasing wavelength. Here we use a 2DH morphodynamic model resolving surf zone instabilities to investigate whether EHAWI could approximate a real instability in nature with a characteristic lenghscale. Assuming very idealized conditions on the bathymetric profile and sediment transport we find a 2DH instability mode consisting of shore-oblique upcurrent bars coupled to a meandering of the longshore current. This mode grows for high-angle waves, above about 30 degrees (offshore) and the maximum growthrate occurs for the angle maximazing the angle at breaking, about 70 degrees (offshore). The dominant wavelength is of the order of the surf zone width. Interestingly, for long sand waves the growth rate never becomes negative and it matches very well the anti-diffusive behaviour of EHAWI. This distinguishes the present instability mode from other modes found in previous studies for other bathymetric and sediment transport conditions. Thus we conclude that EHAWI approximates a real morphodynamic instability only for quite particular conditions. In such case, a characteristic length scale of the instability emerges thanks to surf zone processes that damp short wavelengths.

Ocean Dynamics manuscript No.
(will be inserted by the editor)

A New Instability Mechanism Related to High-Angle Waves

Albert Falqués · Nabil Kakeh · Daniel Calvete

Received: date / Accepted: date

Abstract For wave incidence angles at breaking above $\approx 45^\circ$ the one-line approximation of coastal dynamics predicts an unstable shoreline giving rise to the formation of self-organized sand waves. This instability (EHAWI) is scale-free and

A. Falqués

Physics Department, Universitat Politècnica de Catalunya, Campus Nord UPC, C. Jordi Girona 1-3, 08034 Barcelona, Catalonia, Spain

Tel.: +34-934016889

Fax: +34-934016090

E-mail: albert.falques@upc.edu

N. Kakeh

Physics Department, Universitat Politècnica de Catalunya, Campus Nord UPC, C. Jordi Girona 1-3, 08034 Barcelona, Catalonia, Spain

E-mail: nabil.kakeh@upc.edu

D. Calvete

Physics Department, Universitat Politècnica de Catalunya, Campus Nord UPC, C. Jordi Girona 1-3, 08034 Barcelona, Catalonia, Spain

E-mail: daniel.calvete@upc.edu

the growthrate increases without bound for decreasing wavelength. Here we use a 2DH morphodynamic model resolving surf zone instabilities to investigate whether EHAWI could approximate a real instability in nature with a characteristic lenghscale. Assuming very idealized conditions on the bathymetric profile and sediment transport we find a 2DH instability mode consisting of shore-oblique upcurrent bars coupled to a meandering of the longshore current. This mode grows for high-angle waves, above about 30° (offshore) and the maximum growthrate occurs for the angle maximazing the angle at breaking, about 70° (offshore). The dominant wavelength is of the order of the surf zone width. Interestingly, for long sand waves the growth rate never becomes negative and it matches very well the anti-diffusive behaviour of EHAWI. This distinguishes the present instability mode from other modes found in previous studies for other bathymetric and sediment transport conditions. Thus we conclude that EHAWI approximates a real morphodynamic instability only for quite particular conditions. In such case, a characteristic length scale of the instability emerges thanks to surf zone processes that damp short wavelengths.

Keywords coastal geomorphology · self-organized patterns · high-angle waves · shore-oblique sand bars

PACS 92.10.Sx · 92.10.Wa

1 Introduction

The shorelines of sandy coasts are hardly straight but quite often display undulations at various lengthscales. These undulations are sometimes relatively regular or even nearly alongshore periodic with a wavelength λ, suggesting that they are

the imprint of a physical mechanism dominating the dynamics of this stretch of coast with λ being its characteristic length scale. Perhaps the most known are beach cusps that may develop at the swash zone and typically have horn-to-horn distances of $\lambda \sim 1 - 50$ m Almar et al (2008). At a larger scale, shorelines may display undulations with a wavelength in the range $\lambda \sim 100 - 1000$ m that are known as megacusps. They are linked to crescentic bars, to transverse bars or, more generally, to rip channel systems Orzech et al (2011). In case of transverse bars, their apexes develop at the shore attachements of the bars and the embayments in between correspond to the troughs in between bars. Megacups can also form due to the influence of a crescentic bar on the circulation and the waves shoreward of it Ribas et al (2015). Finally, shorelines may display undulations at a scale which is even larger than surf zone rhythmic bars, i.e., $\lambda \gg X_b$, where X_b is the width of the surf zone. These large scale undulations have typical alongshore wavelengths $>$ 1km (on open ocean beaches) and are linked to similar undulations in the depth contours well offshore the surf zone. They have been called km-scale shoreline sand waves (Idier and Falqués, 2014).

Shoreline features may be forced by external templates in the hydrodynamics (waves and currents) or by the antecedent geological constraints. However, they can also be self-organized, that is, they can emerge out of the internal dynamics of the coastal system Coco and Murray (2007). In this case the wavelength, λ, and the particular pattern both in the morphology and the hydrodynamics are not dictated by the external forcing but by the internal dynamics. The common approach to understand the emergence of self-organized patterns is as follows. A basic steady equilibrium state without the pattern is assumed. Then an arbitrary perturbation of the morphology is introduced. This causes an alteration of the

hydrodynamics, hence of sediment transport. The gradients in sediment transport create areas of deposition and areas of erosion. If the bathymetric changes reinforce the initial perturbation a positive feedback occurs and the perturbation both in the morphology and in the hydrodynamics will grow. The initial perturbation can in fact be either in the morphology or in the hydrodynamics or in both. This can be studied mathematically by doing the stability analysis of the basic equilibrium state and the emerging patterns are the instability modes. This approach allows understanding the formation of beach cusps Coco et al (2000); Dodd et al (2008), crescentic bars Deigaard et al (1999); Falqués et al (2000); Calvete et al (2005) and transverse bars Ribas et al (2003); Garnier et al (2006); Ribas et al (2012).

The dynamics of wave-dominated sandy shorelines at large length scales $\gg X_b$ can be described with the one-line approximation (see, e.g., Komar, 1998) in which the surf zone collapses in one line (the shoreline). The changes in shoreline position are then governed by the alongshore gradients in the total alongshore sediment transport rate, Q (total volume per time unit). In this context and as it is shown in Figure 1, a cuspate foreland will cause gradients in Q and it will grow if Q decreases moving from the updrift side (A) to the downdrift side of the apex (B). The sediment transport rate is commonly computed with semi-empirical formulae (e.g., the CERC formula Komar, 1998) and depends on the wave height H_b and on the angle between wave fronts and local shoreline at breaking, α_b:

$$Q = Q(H_b, \alpha_b) \tag{1}$$

The Q function increases with H_b but regarding the angle it is increasing up to a critical angle $\alpha_{bc} \sim 45^\circ$ and it is decreasing for $\alpha_b > \alpha_{bc}$. Then, assume first that the shoreline undulation do not affect the bathymetric contours that

keep on being rectilinear and parallel to the undisturbed shoreline. In this case, H_b does not change along the shore. Let us also assume $\alpha_b > \alpha_{bc}$, i.e., Q is decreasing by increasing α_b. Since the wave angle (relative to the local shoreline) increases moving from updrift of the apex (A) to downdrift of it (B), Q will decrease so that the cuspate foreland will grow (situation shown in Figure 1). On the contrary, if the angle is below the critical value, $\alpha_b < \alpha_{bc}$, the cuspate foreland will decay. This is a first type of instability, which will be referred to as EHAWI (the motivation for this term is explained later on). Although it was first proposed a long time ago by Zenkovitch (1959) it has been largely ignored because, due to bathymetric refraction, the wave angle at breaking hardly reaches the critical one, $\alpha_{bc} \simeq 45^\circ$. However, the depth contours tend to deform following the undulation of the shoreline. As a result there are differences in refractive wave crest stretching between updrift (A) and downdrift (B) so that H_b tends to be larger updrift than downdrift. This makes Q to be larger at (A) so that it favors instability that would then occur for angles $\alpha_b < \alpha_{bc}$. Studying this second option requires defining a link between the shoreline undulations and the bathymetric undulations and it is found that shoreline instability occurs for $\alpha_0 > \alpha_{0c}$, where α_0 is the wave angle at the depth of closure, D_c, that is, the maximum depth where the shoreline undulation can be noticed in the depth contours. It turns out that $\alpha_{0c} \sim \alpha_{bc}$. This second type of instability is more plausible as wave angles at D_c can be much larger than at breaking. We call it HAWI (High-angle wave instability) after Ashton et al (2001) and it has been extensively studied in recent years Ashton et al (2001); Falqués and Calvete (2005); Ashton and Murray (2006); Medellín et al (2009); Ashton et al (2009); van den Berg et al (2012); Kaergaard and Fredsoe (2013); Idier and Falqués (2014).

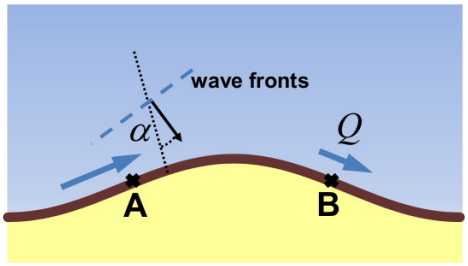

Fig. 1 Alongshore distribution of total sediment transport rate leading to the growth of a sandy cuspate foreland. The definition of the wave angle α relative to the local shoreline orientation is shown.

The aim of the present contribution is investigating the instability associated to a large wave angle at breaking. Hereinafter it will referred to as EHAWI (Extreme high-angle wave instability). The essential difference between both instabilities is that HAWI is associated to a link between the surf and shoaling zones while EHAWI is just related to the surf zone. We will show that the one-line framework predicts an unrealistic behaviour of the instability at relatively short wavelengths, $\lambda \sim X_b$. By this reason, we will then use a 2DH (two horizontal dimensions) stability model to explore the instability in a more realistic context. Under some conditions we will find a 2DH instability mode sharing some of the characteristics of EHAWI.

2 One-line approach

Let us assume a Cartesian coordinate system with y along the unperturbed shoreline, x normal to it pointing seawards and z vertical upwards. According to sediment conservation, the governing equation for the perturbed shoreline, $x_s(y,t)$, is

Komar (1998)

$$\frac{\partial x_s}{\partial t} = -\frac{1}{D_c}\frac{\partial Q}{\partial y} \tag{2}$$

If θ is the absolute wave angle with respect to the unperturbed shoreline and ϕ is the angle of the local shoreline orientation with respect to the y axis, the relative wave angle is $\alpha = \theta - \phi$. Then, under the assumption that shoreline undulations do not affect the wave field, $\partial H_b/\partial y = 0, \partial \alpha_b/\partial y = 0$ it follows

$$\frac{\partial Q}{\partial y} = \frac{\partial Q}{\partial \phi}\frac{\partial \phi}{\partial y} = -\frac{\partial Q}{\partial \alpha}\frac{\partial \phi}{\partial y} \tag{3}$$

Thus, under the assumption of small shoreline undulations, $\partial x_s/\partial y = \tan\phi \approx \phi$ and a diffusion equation follows as governing equation Pelnard-Considère (1956)

$$\frac{\partial x_s}{\partial t} = \epsilon \frac{\partial^2 x_s}{\partial y^2} \tag{4}$$

with

$$\epsilon = \frac{1}{D_c}\frac{\partial Q}{\partial \alpha} \tag{5}$$

being the diffusivity. For $\theta_b > \theta_{bc}$, $\partial Q/\partial \alpha < 0$ and the diffusivity is negative. In this case, the shoreline is unstable as can be seen by examining a small amplitude undulation of the form:

$$x_s(y,t) = Ae^{\sigma t + iKy} + c.c. \tag{6}$$

where c.c. means complex conjugate, A is a constant small amplitude, σ is the complex growthrate and $\lambda = 2\pi/K$ is the wavelength. By inserting eq. 6 into the governing equation, eq. 4, the growthrate follows:

$$\sigma = -\epsilon K^2 \tag{7}$$

and it is seen that it is positive for $\epsilon < 0$.

In case of using the CERC formula Komar (1998),

$$Q = \mu H_b^{5/2} \sin(2\alpha_b) \tag{8}$$

$\alpha_{bc} = 45^\circ$ and the diffusivity,

$$\epsilon = \frac{2\mu}{D_c} \cos(2\alpha_b) \tag{9}$$

is clearly negative for $\alpha_{bc} > 45^\circ$.

It is remarkable that the growth rate increases without bound for decreasing wavelength, λ, so that there is no characteristic lengthscale of the instability. But more importantly, these so large growthrates for short wavelengths are unrealistic and nonsense since the one-line approach is not applicable at the lenghscale of the surf zone, X_b, or smaller. Therefore, it is plausible that the surf zone processes which are not resolved by the one-line approach dominate the instability at those short lenghscales. Moreover, although the one-line approximation predicts an unstable shoreline for $\theta_b > \theta_{bc}$ this approximation is a very crude representation of reality. Therefore, it remains unknown whether the instability will still be present if the surf zone processes are included in the modelling.

3 2DH stability model

To investigate i) whether the shoreline instability is not an artifact of the one-line approximation and it still exists in a 2DH frame (two horizontal dimensions) and ii) if there is a characteristic lengthscale of the instability, we use the morfo60 linear stability model describing the coupling between waves, depth-averaged currents and bathymetric changes in the surf zone with 2 horizontal dimensions. The model is described in more detail in Calvete et al (2005) and Ribas et al (2012) and here

we only revisit the main features. The coordinate system defined in section 2 is used but, as needed, (x_1, x_2) will stand for (x, y). The shoreline is formally fixed ($y = x_2 = 0$) in this model, but a shoal (deep) developing near the shoreline can be physically interpreted as a shoreline progradation (retreat).

3.1 Waves

Waves are assumed to have a narrow spectrum in frequency and angle. Their heights are supposed to follow the Rayleigh distribution, characterized by the root mean square wave height, H_{rms} (wave energy being $E = \rho g H_{rms}^2/8$, where ρ is the water density and g is gravity). When they approach the coast, their transformation is described using linear wave theory, which yields expressions for the wave properties such as the radiation stresses, S_{ij}^w, the root mean square wave orbital velocity amplitude, u_{rms}, and the two components of the group and phase velocity, c_{gi} and c_i, respectively. The dispersion relation reads

$$\omega = \sqrt{g|\nabla\Phi| \tanh(D|\nabla\Phi|)} + v_j \frac{\partial\Phi}{\partial x_j} \tag{10}$$

where ω is the absolute frequency and the Doppler shift is accounted for. In this equation and hereinafter, dummy indices are assumed to be summed, e.g., over $j = 1, 2$. Here, Φ, is the phase, from where the wavenumber and the wave angle are computed through $k_i = \partial\Phi/\partial x_i$. The two components of the depth-averaged fluid velocity are v_i, $D = z_s - z_b$ is the water depth, where z_s is the mean free surface level, and z_b is the sea bed level. Steady conditions are assumed, $\omega =$ constant. This equation describes the refraction and shoaling of the waves due to both topography and currents. More complex processes in wave propagation, like wave diffraction, are not accounted for.

Wave energy balance is described with a wave- and depth-averaged equation (with wave-current interactions),

$$\frac{\partial E}{\partial t} + \frac{\partial}{\partial x_j}\left((v_j + c_{gj})E\right) + S^w_{jk}\frac{\partial v_k}{\partial x_j} = -\mathcal{D}_w \tag{11}$$

where the wave energy dissipation $\mathcal{D}_w$ is computed with the Church and Thornton (1993) formulation. The energy dissipated by breaking feeds the surface rollers, i.e. the aerated mass of water located on the shoreward face of breaking waves. The wave- and depth-averaged roller energy balance is

$$2\frac{\partial E_r}{\partial t} + 2\frac{\partial}{\partial x_j}\left((v_j + c_j)E_r\right) + S^r_{jk}\frac{\partial v_k}{\partial x_j} = -\mathcal{D}_r + \mathcal{D}_w \tag{12}$$

where E_r is the energy of the rollers, S^r_{ij} are the radiation stresses due to roller propagation and $\mathcal{D}_r$ is the roller energy dissipation rate. Given $\omega = 2\pi/T_p$, H_{rms} and θ at the offshore boundary, equations 10, 11 and 12 allow computing k, θ and H_{rms} in the whole domain.

3.2 Mean hydrodynamics

The mean fluid motions are governed by the wave- and depth-averaged mass and momentum balance equations, where the radiation stresses due to both wave and roller propagation are included,

$$\frac{\partial D}{\partial t} + \frac{\partial}{\partial x_j}\left(Dv_j\right) = 0 \tag{13}$$

$$\frac{\partial v_i}{\partial t} + v_j\frac{\partial v_i}{\partial x_j} = -g\frac{z_s}{x_i} - \frac{1}{\rho D}\frac{\partial}{\partial x_j}\left(S^w_{ij} + S^r_{ij} - S^t_{ij}\right) - \frac{\tau_{bi}}{\rho D} \quad , \qquad i = 1, 2 \tag{14}$$

and where, τ_{bi} are the bed shear stresses. The turbulent Reynolds stresses are S^t_{ij} and they are modelled with the standard eddy viscosity approach. The lateral turbulent mixing coefficient is directly linked to the roller energy dissipation, $\mathcal{D}_r$

(the main source of turbulence), $\nu_t = M(\mathcal{D}_r/\rho)^{1/3}$, where $M = 1$. The fluid velocities are imposed to be zero at both the coastline and the offshore boundary. Also, the free surface elevation is zero at the offshore boundary.

3.3 Sediment transport and bed updating

Conservation of sediment mass yields the bottom evolution equation

$$(1-p)\frac{\partial z_b}{\partial t} + \frac{\partial q_j}{\partial x_j} = 0 \tag{15}$$

with $p = 0.4$ being the porosity of the bed and q_j the two components of the wave- and depth-averaged volumetric sediment transport (m^2/s). A widely accepted formulation for q_j in the nearshore is that of Soulsby (1997). Their original expression has been extended to model the effect of a 2-dimensional flow and the preferred downslope transport of the sand,

$$q_i = C\left(v_i - \Gamma\frac{\partial h}{\partial x_i}\right) \quad , \qquad i = 1,2 \tag{16}$$

where C is the depth-integrated volumetric sediment concentration. The bed slope term, proportional to Γ, accounts for the tendency of the system to smooth out the sea bed perturbations, h, if the latter would not cause a positive feedback into the flow. The sediment concentration, C, is a function of the current, the wave orbital velocity and the roller energy dissipation. However, since we want to seek the instability suggested by the one-line modelling, we will assume C =const. to avoid introducing specific features of 2DH formulations that would not be represented in the one-line approximation.

3.4 Linear stability analysis

The equations 10, 11, 12, 13, 14 and 15, which govern this morphodynamic system, together with the parameterizations used and the appropriate boundary conditions, define a closed dynamical system for the variables $v_1, v_2, z_s, E, E_r, \Phi$ and z_b. The stability analysis starts by defining a steady and alongshore uniform basic state (i.e., without the alongshore rhythmic patterns), which is defined by an equilibrium beach profile, $z_b = z_{b0}(x)$, and the wave parameters at the offshore boundary, H_{rms}, T_p and θ at the offshore boundary. The modeled basic state is characterized by the presence of a longshore current, $v_{01} = 0$ and $v_{02} = V_0(x)$, and an elevation of the mean sea level, $z_{s0} = z_{s0}(x)$. This basic state represents a morphodynamic equilibrium only under the assumption that the net cross-shore sediment flux is zero. Once the variables in the basic state are computed, a perturbed state of the form

$$(v_1, v_2, z_s, E, E_r, \Phi, z_b) = (\ 0, V_0, z_{s0}, E_0, E_{r0}, \Phi_0, z_{b0}) + e^{\ \sigma t + iKy}(u, v, \eta, \hat{e}, \hat{e}_r, \phi, h) \ + \ c.c. \qquad (17)$$

is assumed, where the superscript 0 stands for the basic state variables.

By inserting equation 17into the governing equations 10-2 and linearizing with respect to the perturbations, an eigenproblem is obtained where σ is the eigenvalue and $(u(x), v(x), z_s(x), \hat{e}(x), \hat{e}_r(x), \phi(x), h(x))$ are the eigenfunctions. For each perturbation wave number, $K = 2\pi/\lambda$, a number of eigenvalues σ with the corresponding eigenfunctions exist, which characterize the different growing (or decaying) modes. The growth rate of the emerging features is given by $\sigma_r = \Re e(\sigma)$, so that $\sigma_r > 0$ means growth. In case of an unstable basic state, solutions with $\sigma_r > 0$ are found and the instability curves show these positive σ_r for different values of

K. Starting from arbitrary small initial perturbations, the dynamics after some time will be dominated by the mode with largest growth rate, which is called Fastest Growing Mode (FGM). Its characteristic growth time (e-folding growth time) is given by σ_r^{-1} and the alongshore migration speed by $c = -\Im m(\sigma)/K$. The possible emerging patterns in the wave field, the mean hydrodynamics and the morphology are defined by the eigenfunctions corresponding to the growing modes.

4 2DH stability computations

4.1 Basic state

For the sake of simplicity and keeping as close as possible to the one-line approach, we use a planar reference beach profile, $z_{b0}(x) = -\beta x$, with $\beta = 0.02$. We assume $H_{rms}^{off} = 1$ m and $T_p = 6$ s at $D_{off} = 20.3$ m. Wave angles at D_{off} are explored from $\theta_{off} = 0$ to $\theta_{off} = 90^\circ$. The depth integrated sediment concentration is $C = 0.002$ m. Regarding the bed slope coefficient, the values $\Gamma = 0.1, 0.01, 0.001$ and 0 m/s will be explored. The characteristics of the basic state for $\theta_{off} = 70^\circ$ are shown in Figure 2. A maximum current of $V_m \approx 0.7$ m/s at $x \approx 40$ m is found. For irregular waves, a single breaking point does not exist and hence there is not a well defined width of the surf zone. Here we define an "effective breaking point" as the cross-shore position, $x = X_b$, where $3H_{rms} = \gamma_b D$. As can be seen, almost all the longshore current profile fits into $0 \leq x \leq X_b$, which means that this is approximately the region where the longshore transport takes place. Thus, this is the alongshore strip that can be considered to collapse into the shoreline in the one-line approach. Moreover, the wave angle at this position is the θ_b that

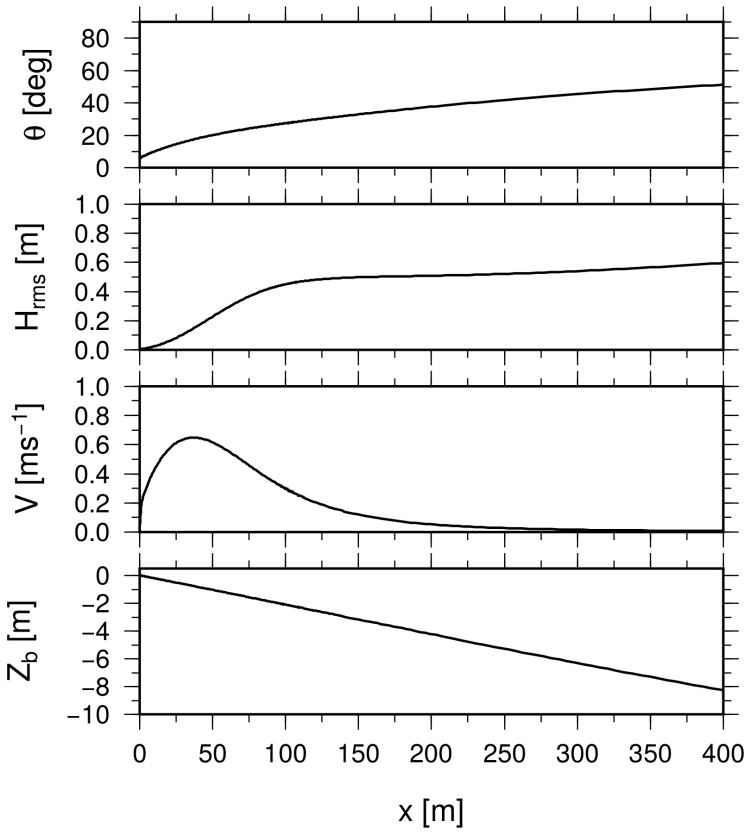

Fig. 2 Basic state for the instability analysis, for $T_p = 6$ s, $\theta_{off} = 70°$ and $H_{rms}^{off} = 1$ m.

could be compared with the corresponding angle for the one-line approximation. For this case the surf zone width is $X_b \approx 190$ m and the wave angle at breaking is $\theta_b \approx 37°$. The values $\beta = 0.02, T_p = 6$ s and $D_{off} = 20.3$ m will be used as default in all the study.

4.2 Instability mode for high-angle waves

Wavelengths in the range $\lambda = 0 - 1000$ m are explored. To keep our 2DH analysis close to the one-line approach the bed-slope transport should be switched off by taking $\Gamma = 0$. In this case however many spurious unstable modes appear (purely

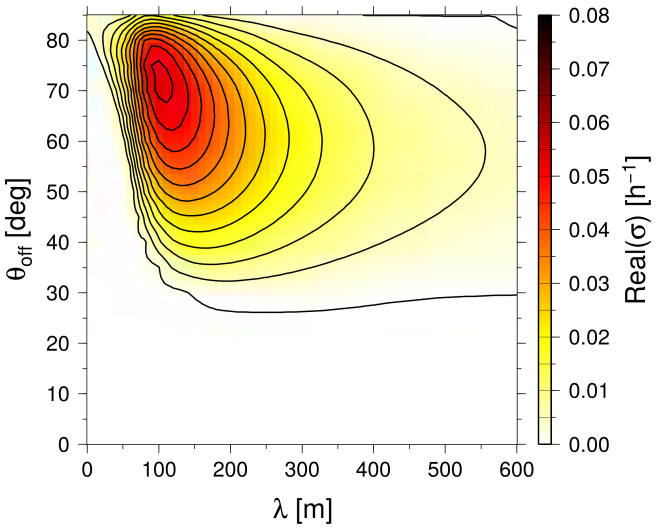

Fig. 3 Contour lines of instability growth rate as a function of the alongshore wavelength, λ, and the offshore wave angle, θ_{off}, for $H_{off} = 1$ m.

numerical eigenvalues, see, e.g., Calvete et al, 2005) and physically reliable solutions cannot be identified. On the contrary, for $\Gamma = 0.1, 0.01, 0.001$ m/s only one growing instability mode is found in the $\lambda = 0 - 1000$ m range. This mode is qualitatively very similar for the different Γ values and it therefore seems that it converges in the limit $\Gamma \to 0$. Here we discuss the results of the $\Gamma = 0.01$ m/s case, which are therefore representative of such limit.

Interestingly and as it is shown in Figure 3, the instability develops only for $\theta_{off} > 30°$. Its maximum intensity occurs for $\theta_{off} \approx 70°$ with a characteristic growth time $\sigma_r^{-1} \approx 18$ h and a wavelength $\lambda \approx 105$ m. The downdrift migration celerity is $c \approx 8$ m/h. The instability curve of the growing mode for $\theta_{off} = 70°$ is shown in Figure 4. It is seen that this mode grows only for $\lambda > 50$ m, the maximum growth occurs for $\lambda \approx 105$ m and for $\lambda \approx 1000$ m the growth rate becomes negligible. The perturbed depth contours (Figure 5) correspond to wide

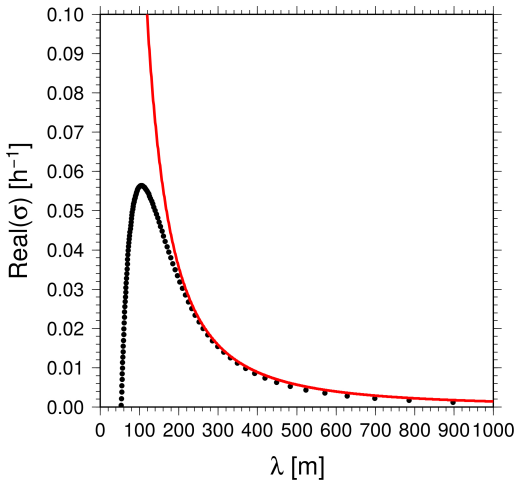

Fig. 4 Instability curves for: EHAWI with the one-line approximation (eq. 7) for $\epsilon = -0.01$ $m^2 s^{-1}$ (red thick line) and for the 2DH instability mode with $\theta_{off} = 70°$ (black dotted line).

oblique bars that are upcurrent-oriented, that is, the distal tip of the bars are shifted updrift with respect to the shore-attachment (Ribas et al, 2015). Although the model does not describe it explicitly, at the shore attachment of the bars a megacusp would develop in reality and shoreline embayments would occur where the troughs meet the shoreline. Coupled to the growing morphology there is a meandering in the longshore current so that the current veers seaward updrift of the bars and shoreward downdrift of the bars. The maximum current intensity occurs at the lee of the bars. At large wavelengths this mode also grows but much more slowly. For example, for $\lambda = 900$ m the characteristic growth time is 36 d. As shown in Figure 6, in this case it displays long bathymetric undulations and the bars are hardly visible.

To get more insight into the relation between EHAWI and the 2DH instability mode, the growth rate corresponding to EHAWI for the one-line modelling, $\sigma = -\epsilon(2\pi/\lambda)^2$ (eq. 7) is also plotted in Figure 3. It is remarkable that by chosing

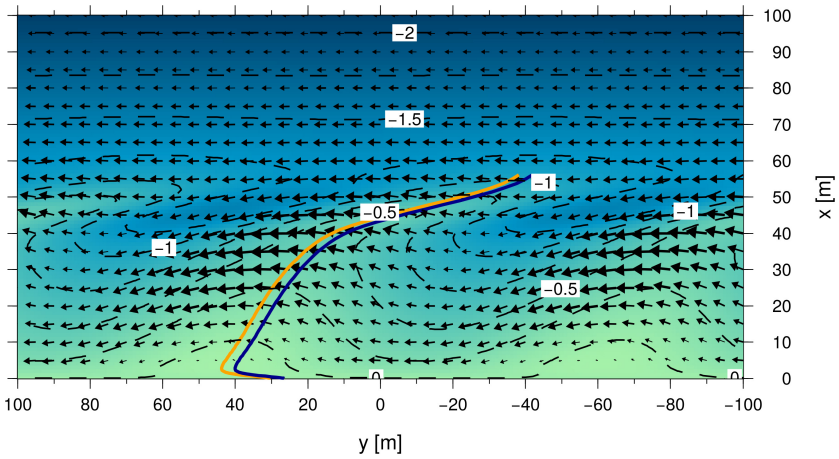

Fig. 5 Perturbed bathymetry and longshore current corresponding to the instability mode for $\theta_{off} = 70°$ and for the dominant wavelength, $\lambda = 105$ m (2 wavelengths are shown). An arbitrary amplitude for the perturbation has been chosen to ease visualization. The shore is at the bottom of the plot and the wave incidence is from the right. Deep blue color represents deeper areas while lighter colors represent shallower areas. The yellow line indicates the crest of a bar, $y = F(x, y_0)$. The blue line is the line parallel to the bar crest with maximum total sediment transport rate across it, $Q^*(y)$.

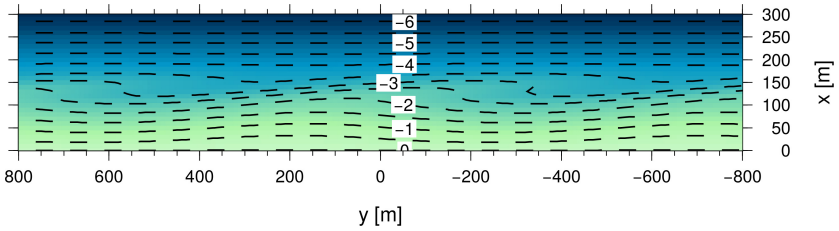

Fig. 6 Bathymetric pattern of the instability mode for $\theta_{off} = 70°$ for a large wavelength, $\lambda = 900$ m. An arbitrary amplitude for the perturbation has been chosen. The shore is at the bottom of the plot and the wave incidence is from the right. Deep blue color represents deeper areas while lighter colors represent shallower areas.

a diffusivity $\epsilon = -0.01$ m^2 s^{-1}, the tale for long wavelengths of the 2DH instability curve fits very well the EHAWI instability curve. This asymptotic behaviour of the instability curve for long wavelengths (anti-diffusional) distinguishes the present instability from others where the growth rate drops to zero above a given wavelength. This is the case, for example, for crescentic bars Falqués et al (2000); Calvete et al (2005) or transverse bars Ribas et al (2012). This provides confidence on the 2DH mode as being the 2DH counterpart of EHAWI. The fitting value of ϵ is realistic. Indeed, by representing the alongshore transport with the CERC formula with a common value $\mu = 0.2$ m$^{1/2}$ s^{-1} and assuming $H_b = 1$ m, $D_c = 5$ m, the value of $\epsilon = -0.01$ m^2 s^{-1} is obtained for $\theta_b = 47°$.

4.3 Analysis of the longshore sediment transport

To relate the 2DH instability mode with the EHAWI instability coming out of the one-line approach we try to define a magnitude playing the role of the total alongshore transport rate Q but in the 2DH approach. The straightforward option would be the integral of the alongshore sediment flux in any cross-section from the shoreline, $x = 0$, to the offshore boundary, $x = x_{off}$. But since the bathymetric undulations are shifted with respect to the associated shoreline undulation (upcurrent-oriented bars), the alongshore gradients in this magnitude could not be easily linked to the growth/decay of the morphological features contrarily to what happens for Q in the one-line approach. Therefore, consider for each x_0 the crest of a bar as the position of the maximum bed level following alongshore the line $x = x_0$. Then, if $y = f(x)$ is the crest of the bar that attaches at the shoreline at $y = 0$, we define the line which is parallel to that bar crest and meets the shoreline

at $y = y_0$ by (see Figure 7)

$$y = F(x, y_0) = y_0 + f(x) \tag{18}$$

Finally, we define the total sediment transport rate crossing the lines that are parallel to the crests by

$$Q^*(y_0) = \int_0^{s_{off}} \mathbf{q} \cdot \hat{\mathbf{n}}\, ds \tag{19}$$

where the integral is done along the line $y = F(x, y_0)$, $\hat{\mathbf{n}}$ is the normal unit vector to this line pointing downdrift, and s is the length along this line. Thereinafter we will refer to $Q*$ as the total cross-bar sediment transport rate. Let us consider the region $\mathcal{S}$ bounded by two of these lines, $y = F(x, y_1), y = F(x, y_2)$, by the shoreline, $x = 0$, and by the offshore boundary, $x = x_{off}$. Let $y = F(x, y_1)$ and $y = F(x, y_2)$, with $y1 < y2$, be its updrift and downdrift boundaries, respectively. Then, since there is sediment flux only across these two lateral boundaries, if $Q^*(y_1) > Q^*(y_2)$, there will be convergence of sediment in $\mathcal{S}$ so that the mean sea bed in $\mathcal{S}$ will rise on average. Therefore, as in the one-line approach, the morphological feature will grow if Q^* decreases moving from updrift to downdrift of the shoreline apex or, in other words, if the maximum in $Q^*(y)$ is shifted updrift with respect to the apex (between the apex and the updrift embayment). Figure 8 shows that, indeed, this is the case (yet weakly) for the 2DH instability mode and it can therefore be associated to the one-line instability based on the gradients in Q.

5 Discussion

The surf zone morphodynamic instability mode we have found shares most of the essential characteristics of EHAWI:

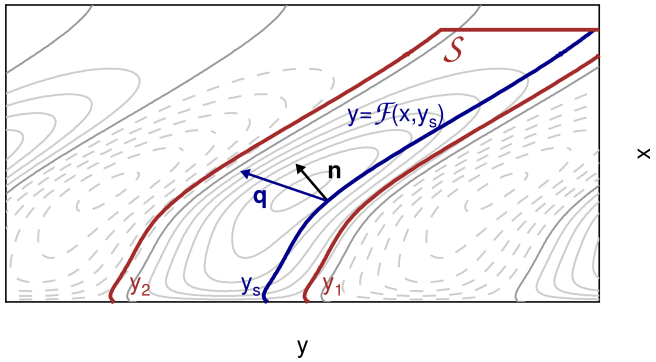

Fig. 7 Control volume $\mathcal{S}$ to analyze the growth or decay of morphological features as a function of the total along-current sediment transport rate, Q^*. Downdrift direction is from right to left. The contour lines of the bed level perturbation are also shown (solid lines correspond to bars, dashed lines correspond to troughs).

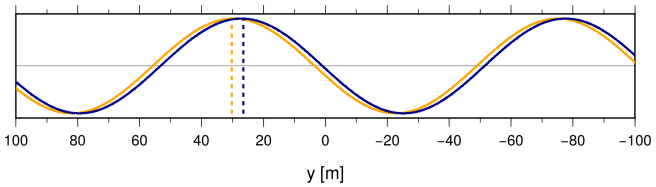

Fig. 8 Alongshore distribution of the alongshore sediment flux (blue line) in comparison with the shoreline undulation (yellow line). Downdrift direction is from right to left.

1. It occurs only above a critical angle $\theta_{off} \sim 30^\circ$ and it has its maximum growth for very high angle waves, $\theta_{off} \sim 70^\circ$.
2. For relatively large wavelengths (in comparison with X_b), the growth rate follows an anti-dffusional behaviour that is fully consistent with the one-line approach. As far as we know, none of the existing studies for surf zone morphodynamic instabilities gives this behaviour.
3. The instability is related to the alongshore gradients in total longshore sediment transport rate, Q^*.

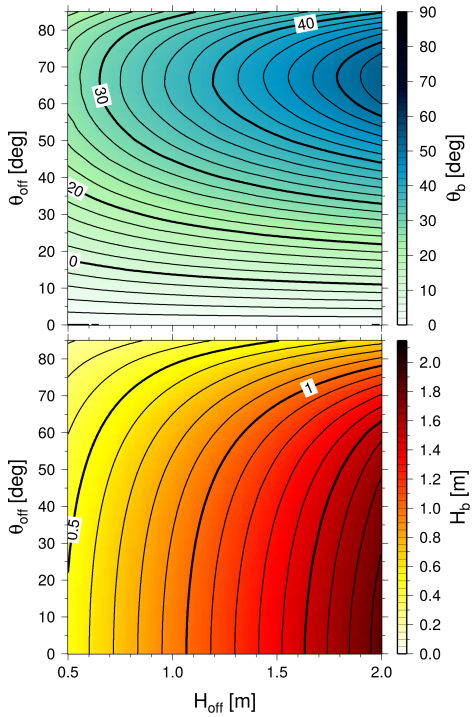

Fig. 9 Wave angle, θ_b, and wave height, H_b, at breaking as a function of offshore wave angle, θ_{off}, and wave height, H_{off}.

4. It does not depend essentially on the coupling between the surf and shoaling zones through cross-shore sediment transport and it develops only in the surf zone.

However, both instabilities are not fully consistent because EHAWI develops only for $\theta_b > 45^\circ$ while the 2DH mode develops for smaller θ_b, above $\theta_b \sim 22^\circ$. It is nevertheless true that the maximum intensity of the instability occurs for an offshore angle $\theta_{off} \approx 70^\circ$, which is the offshore angle that maximizes the angle at breaking (see Figure 9). This clearly suggests that the instability is anyway associated to a large wave angle at breaking.

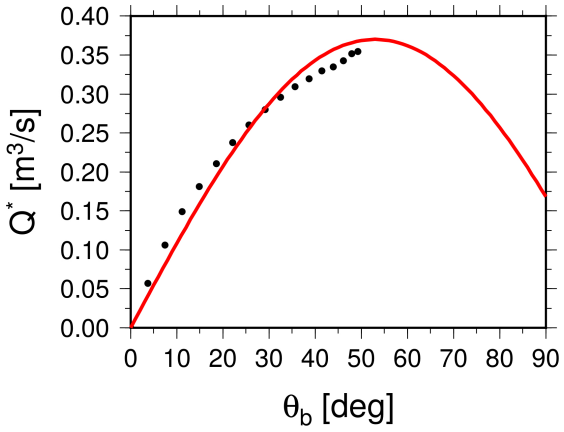

Fig. 10 Dotted line: total alongshore transport rate, Q^*, as a function of wave angle at breaking θ_b for $H_b = 1$ m. Continuous line: fitting with $Q^* = a \sin 2c\theta_b$, where $a = 0.37\mathrm{m}^3/\mathrm{s}$ and $c = 0.85$.

To examine more in depth the consistency between the 2DH instability mode and EHAWI regarding the wave angle at breaking, we first compute the total sediment transport rate Q^* as a function of θ_b for $H_b = $ const. in the 2DH approach (for the basic state). We will look for a wave angle θ_{bc} maximazing Q^* and we will investigate whether the instability depends on θ_b being below or above θ_{bc}. Figure 10 shows Q^* as a function of θ_b for $H_b = 1$ m. The plot has been done by exploring θ_{off} between 0 and 80° and selecting the H_{off} necessary to have $H_b = 1$ m. It is seen that θ_b does not exceed 50° and that there is no maximum of Q^* in this range. However, the Q^* curve can be roughly fitted by $Q^* = a \sin 2c\theta_b$, where $a = 0.37\mathrm{m}^3/\mathrm{s}$ and $c = 0.85$, which means that extrapolating the tendency below 50° would suggest a maximum at $\theta_b \simeq 53°$. But in the range of θ_b that is ferm there is no θ_{bc} and we cannot therefore explore $\theta_b > \theta_{bc}$. Nevertheless, we think it is still worth examining the instability for $\theta_b > 45°$, which is the angle maximazing Q for the one-line approach (CERC formula, eq. 8) to see if there are

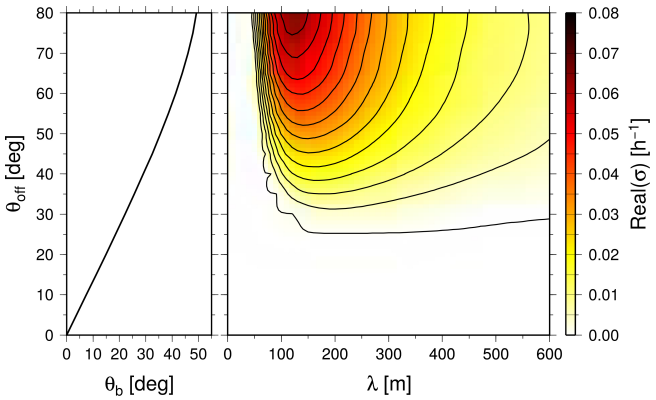

Fig. 11 Right panel: contour lines of instability growth rate as a function of the alongshore wavelength, λ, and the offshore wave angle, θ_{off}, for $H_b = 1$ m. Left panel: offshore wave angle, θ_{off}, as a function of θ_b for $H_b = 1$ m.

significant differences whith the mode found in section 4.2. An instability analysis similar to that done in section 4.2 is persued here, but instead of keeping $H_{off} = 1$ m we now select H_{off} for each wave angle in order to have $H_b = 1$ m. Figure 11 shows the growth rate of the instability as a function of λ and θ_{off} together with θ_b. It is seen that the instability occurs for $\theta_b > 20^\circ$ and θ_b reaches values above 45°. The σ_r contour lines keep on being smooth, i.e., there is no singularity or transition for any particular θ_b value (apart from the lower bound of $\theta_b \approx 20^\circ$). It is also clear that, as a result of keeping $H_b = $ const., the maximum instability occurs now for the maximum angle, both offshore and at breaking (i.e., $\theta_b = 50^\circ$). The dominant wavelength is $\lambda \approx 120$ m. The morphological and hydrodynamic patterns are very similar to that shown in Figure 5. Thus, we conclude that the 2DH instability is related with large wave angle at breaking but θ_b does not need to be above a critical value maximizing Q^* for $H_b = $ const., in contrast with the one-line framework.

On the other hand, surf zone morphodynamic instabilities leading to up-current oriented oblique bars had already been studied Ribas et al (2003, 2012) and the results are quite similar to those for the present 2DH surf zone instability mode. Importantly, the bars in those studies also develop only for quite oblique wave incidence. The gradients in the alongshore transport had not explicitly been examined in the analysis of the formation mechanism but since there is a seaward directed cross-shore component of the meandering current on the bars, mass conservation implies convergence of the longshore component on the bars. However, the new aspect of the present study is the connection with EHAWI in the framework of the one-line approximation and, in particular, the match between both instabilities for large wavelengths that is different from the behaviours previously found Falqués et al (2000); Calvete et al (2005); Ribas et al (2003, 2012). The conclusion would be that there could be a number of different self-organized surf zone rhythmic patterns associated to high-angle waves. The morphology and the specific formation mechanism and, whether they can be related or not to EHAWI, depend on the basic bathymetric profile and wave conditions and, in particular, on the cross-shore distribution of the depth averaged sediment concentration Ribas et al (2015).

6 Conclusions

In the framework of the one-line shoreline modelling self-organized shoreline sand waves without associated bathymetric undulations in the shoaling zone can emerge if the wave angle at breaking is higher than about 45° (EHAWI: extreme high-angle wave instability). This instability is scale-free and has a very unrealistic behaviour

for short wavelengths, the growth-rate increasing without bound for decreasing wavelength. To find out to which extent EHAWI could nevertheless approximate something real in nature, we have used a 2DH linear stability model resolving surf zone morphodynamic instabilities. A single unstable mode growing only for high-angle waves, above a critical offshore angle of about 30° (about 20° at breaking), is found. Its maximum growth rate occurs for the offshore angle maximazing the angle at breaking, (about 70° if offshore wave height is kept constant). The characteristic growth time is about 20 h. It consists of oblique up-current oriented bars with a dominant wavelength of the order of the surf zone width. Its growth is coupled to a meandering in the longshore current and is related to the gradients in alongshore sediment transport. It weakly depends on the diffusive downslope sediment transport and it converges for this transport tending to 0. It can also form with large wavelengths, e.g., $\lambda \approx 900$ m, with a characteristic growth time of 36 days. For large wavelengths the growth rate is never negative and matches very well the anti-diffusional behavior of EHAWI that is found with the one-line approach. It seems therefore that EHAWI would represent the asymptotic behaviour for long wavelengths of this 2DH instability mode. Or, in other words, that the present mode is the 2DH counterpart of EHAWI. Other similar self-organized patterns consisting of up-current oriented bars and occurring for very oblique wave incidence had been obtained in previous studies. The formation mechanisms and their occurrence depend on the bathymetric cross-shore profile, the wave conditions and the sediment transport characteristics. However, none of them match the anti-diffusional bahaviour of EHAWI at large wavelengths. The conclusion is, therefore, that EHAWI do not always represent reality for long wavelengths. It does only for quite particular conditions on bathymetry, waves and sediment

transport. In this case, surf zone processes damp very short sand waves so that a characteristic lenghscale of the order of the surf zone width emerges.

Acknowledgements This research is part of the project CTM2015-66225-C2-1-P funded by the Spanish Government and cofunded by the E.U. (FEDER).

References

Almar R, Coco G, Bryan K, Huntley D, Short A, Senechal N (2008) Video observations of beach cusp morphodynamics. Mar Geol 254:216–223

Ashton A, Murray AB (2006) High-angle wave instability and emergent shoreline shapes: 1. Modeling of sand waves, flying spits, and capes. JGeophysRes 111:F04,011,doi:10.1029/2005JF000,422

Ashton A, Murray AB, Arnault O (2001) Formation of coastline features by large-scale instabilities induced by high-angle waves. Nature 414:296–300

Ashton AD, Murray AB, Littlewood R, Lewis DA, Hong P (2009) Fetch-limited self-organization of elongate water bodies. Geology 37:187–190

Calvete D, Dodd N, Falqués A, van Leeuwen SM (2005) Morphological development of rip channel systems: Normal and near normal wave incidence. J Geophys Res 110(C10006), doi:10.1029/2004JC002803

Church JC, Thornton EB (1993) Effects of breaking wave induced turbulence within a longshore current model. Coastal Eng 20:1–28

Coco G, Murray AB (2007) Patterns in the sand: From forcing templates to self-organization. Geomorphology 91(271-290)

Coco G, Huntley DA, O'Hare TJ (2000) Investigation of a self-organization model for beach cusp formation and development. J Geophys Res 105(C9):21,991–

22,002

Deigaard R, Drønen N, Fredsoe J, Jensen JH, Jørgensen MP (1999) A morphological stability analysis for a long straight barred coast. Coastal Eng 36(3):171–195

Dodd N, Stoker A, Calvete D, Sriariyawat A (2008) On beach cusp formation. J Fluid Mech 597:145–169

Falqués A, Calvete D (2005) Large scale dynamics of sandy coastlines. Diffusivity and instability. J Geophys Res 110(C03007), doi:10.1029/2004JC002587

Falqués A, Coco G, Huntley DA (2000) A mechanism for the generation of wave-driven rhythmic patterns in the surf zone. J Geophys Res 105(C10):24,071–24,088

Garnier R, Calvete D, Falqués A, Caballeria M (2006) Generation and nonlinear evolution of shore-oblique/transverse sand bars. J Fluid Mech 567:327–360

Idier D, Falqués A (2014) How kilometric sandy shoreline undulations correlate with wave and morphology characteristics: preliminary analysis on the Atlantic coast of Africa. Advances in Geosciences 39:55–60, doi:10.5194/adgeo-39-55-2014

Kaergaard K, Fredsoe J (2013) Numerical modeling of shoreline undulations part 1: Constant wave climate. Coastal Eng 75:64–76

Komar PD (1998) Beach Processes and Sedimentation, 2nd edn. Prentice Hall, Englewood Cliffs, N.J.

Medellín G, Falqués A, Medina R, González M (2009) Sand waves on a low-energy beach at 'El Puntal' spit, Spain: Linear Stability Analysis. J Geophys Res 114(C03022), doi:10.1029/2007JC004426

Orzech MD, Reniers AJHM, Thornton EB, MacMahan JH (2011) Megacusps on rip channel bathymetry: Observations and modeling. Coastal Eng 58:890907

Pelnard-Considère R (1956) Essai de theorie de l'evolution des formes de rivage en plages de sable et de galets. In: 4th Journees de l'Hydraulique, Les Energies de la Mer, Paris, Société Hydrotechnique de France, vol III(1), pp 289–298

Ribas F, Falqués A, Montoto A (2003) Nearshore oblique sand bars. J Geophys Res 108(C43119), doi:10.1029/2001JC000985

Ribas F, de Swart HE, Calvete D, Falqués A (2012) Modeling and analyzing observed transverse sand bars in the surf zone. J Geophys Res 117(F02013), doi:10.1029/2011JF002158

Ribas F, Falqués A, de Swart HE, Dodd N, Garnier R, Calvete D (2015) Understanding coastal morphodynamic patterns from depth-averaged sediment concentration. Rev Geophys 53, doi:10.1002/2014RG000457

Soulsby RL (1997) Dynamics of Marine Sands. Thomas Telford, London, U.K.

van den Berg N, Falqués A, Ribas F (2012) Modelling large scale shoreline sand waves under oblique wave incidence. J Geophys Res 117(F03019), doi:10.1029/2011JF002177

Zenkovitch VP (1959) On the genesis of cuspate spits along lagoon shores. J Geol 67:269–277